

# Efficient implementation of the IQA energy partition of the second order Møller-Plesset energy

José Luis Casalz-Sainz<sup>a</sup>, José Manuel Guevara-Vela<sup>b</sup>, Evelio Francisco<sup>a</sup>, Tomás Rocha-Rinza<sup>b</sup>, Ángel Martín Pendás<sup>a,\*</sup>

<sup>a</sup>*Department of Analytical and Physical Chemistry, University of Oviedo, E-33006, Oviedo, Spain.*

<sup>b</sup>*Institute of Chemistry, National Autonomous University of Mexico, Circuito Exterior, Ciudad Universitaria, Delegación Coyoacán C.P. 04510, Mexico City, Mexico.*

---

## Abstract

We describe an efficient implementation of the partition of the second-order Møller–Plesset (MP2) correlation energy within the Interacting Quantum Atoms (IQA) energy decomposition. We simplify the IQA integration bottleneck by considering only the occupied to virtual elements of the second order reduced density matrix, a procedure which reduces substantially the size of the two-electron matrix which has to be addressed. The algorithmic improvements described herein allow to perform the decomposition of the MP2 correlation energy for medium size molecular systems using moderate computational resources. We expect that the methods developed in this investigation will prove useful to understand electron correlation effects through a real space perspective.

*Keywords:*

Electronic correlation, Interacting quantum atoms, MP2

---

## Introduction

The Interacting Quantum Atoms (IQA) [1, 2] approach is an exact partition of the electronic energy based on the exhaustive separation of the real space into disjoint regions as proposed by Bader in the Quantum Theory of Atoms in Molecules (QTAIM). [3] The main advantages of IQA lie in (i) its recovery of the energy of an atom or group of atoms in a

---

\*To whom correspondence should be addressed: [ampendas@uniovi.es](mailto:ampendas@uniovi.es)

molecule or molecular cluster, (ii) its independence from any external reference and (iii) the direct access to the interaction energy between two atoms or groups within a molecule. The last-mentioned circumstance has provided many useful insights about the energetic relationship among the constituents of a system. Indeed, the IQA procedure has been widely successful in the examination of a large variety of chemical problems such as intra- and intermolecular hydrogen bonds, [4–8] the nature of halogen bonding [9–11] or dihydrogen interactions [12], the character of chemical bonding in excited states [13–15], and the description of the metal-ligand interplay in coordination complexes [16, 17]. Additionally, the IQA analysis has been applied to study the role of water clusters in the production of acid rain [18], to examine non-classical contributions in lone pair- and anion- $\pi$  interactions [19, 20], and lately to determine [21] and quantify [22] the spatial localization of the electronic correlation within a chemical bond or to shed light on the nature of chalcogenide bonds.[23] Despite these successful applications, the exploitability of IQA has been limited by its associated computational cost, especially for correlated wave functions. We have recently included dynamical electron correlation in the IQA method by considering either coupled-cluster (CC) and Hartree-Fock (HF) transition density matrices [24] or CC Lagrangians. [25] There have been also implementations of IQA coupled with Møller-Plesset density functions. [26, 27] Because dynamical correlation occupies partially most of the orbitals of the Fock space of a system, and the number of IQA two-electron integrals scales with the fourth power of this set, IQA calculations based on post-HF wavefunctions are still unfeasible for basis sets comprised of more than a few hundred orbitals.

Given the importance of electronic dynamical correlation in the correct description of many chemical and physical phenomena, [28] its inclusion in the IQA methodology at an attainable computational cost is highly desirable. In this contribution, we present an efficient implementation of the IQA partition of the MP2 electronic energy at a relatively moderate computational cost by exploiting the simplified occupied to virtual nature of excitations at the MP level. Overall, we show that this implementation provides a path to study larger electronic systems than those commonly addressed with the IQA analysis for which electron

correlation plays an important role.

## Methodology

The IQA energy partition considers the one- and two-domain division of the non-relativistic Born-Oppenheimer electronic energy [1] as described by the following equation:

$$\begin{aligned}
 E &= \sum_A E_{\text{self}}^A + \sum_{A>B} E_{\text{int}}^{\text{AB}} \\
 &= \sum_A T^A + V_{\text{ne}}^{\text{AA}} + V_{\text{ee}}^{\text{AA}} + \sum_{A>B} V_{\text{nn}}^{\text{AB}} + V_{\text{ne}}^{\text{AB}} + V_{\text{ne}}^{\text{BA}} + V_{\text{ee}}^{\text{AB}}, \quad (1)
 \end{aligned}$$

wherein  $E_{\text{self}}^A$  and  $E_{\text{int}}^{\text{AB}}$  are the IQA self and interaction energies of atom A and pair of atoms AB, while  $T^A$  is the contribution to the kinetic energy of atom A. The terms  $V_{\text{ne}}^{\text{AB}}$  and  $V_{\text{ee}}^{\text{AB}}$  stand respectively for (i) the attraction between the nucleus of domain A and the electrons of atom B and (ii) the repulsion of the electrons in domains A and B. Finally,  $V_{\text{nn}}^{\text{AB}}$  indicates the repulsion between the nuclei in basins A and B.

By further separating the electronic repulsion into its Coulombic and exchange-correlation components we can achieve additional understanding about the nature of the interaction between two atoms, by dividing their interaction energy into classical (coulombic) and exchange-correlation contributions, i.e.,

$$E_{\text{int}}^{\text{AB}} = V_{\text{cl}}^{\text{AB}} + V_{\text{xc}}^{\text{AB}}. \quad (2)$$

The HF approximation considers only Fermi correlation, which is equivalent to the condition  $V_{\text{xc}}^{\text{AB}} = V_{\text{x}}^{\text{AB}}$ , with the RHS of equation (2) having only the exchange term. Møller-Plesset perturbation theory adds correlation corrections directly on top of this HF reference,  $E(\text{MP}) = E(\text{HF}) + E_{\text{corr}}$ . Thus, partitioning  $E_{\text{corr}}(\text{MP})$  à la IQA will then lead to IQA/MP correlation contributions. For the sake of brevity, we will only show how to proceed for the case of second-order corrections (MP2) for closed shell systems, but the following treatment is analogous to the general MPn case.

We can partitionate the MP2 energy,  $E(\text{MP2})$ , as the sum:

$$E = E(\text{HF}) + E_{\text{corr}}^{\text{MP2}} \quad (3)$$

$$= \sum_{pq} D_{pq}^{\text{eff}} h_{pq} + \frac{1}{2} \sum_{pqrs} d_{pqrs}^{\text{eff}} g_{pqrs} + V_{nn}. \quad (4)$$

Wherein  $D_{pq}^{\text{eff}}$  and  $d_{pqrs}^{\text{eff}}$  are effective one and two electron density matrices for the calculation of MP2 energy. In turn, the quantities  $h_{pq}$  and  $g_{pqrs}$  are the mono- and bielectronic integrals:

$$h_{pq} = \int \phi_p^*(\mathbf{r}_1) \left( -\frac{1}{2} \nabla_1^2 - \sum_A \frac{Z_A}{r_{A1}} \right) \phi_q(\mathbf{r}_1) d\mathbf{r}_1, \quad (5)$$

$$g_{pqrs} = \int \int \frac{\phi_p^*(\mathbf{r}_1) \phi_q^*(\mathbf{r}_2) \phi_r(\mathbf{r}_1) \phi_s(\mathbf{r}_2)}{r_{12}} d\mathbf{r}_1 d\mathbf{r}_2, \quad (6)$$

respectively.

We consider the closed-shell expression for  $E_{\text{corr}}^{\text{MP2}}$ ,

$$E_{\text{corr}}^{\text{MP2}} = \sum_{iajb} \frac{2g_{iajb} - g_{ibja}}{\epsilon_i + \epsilon_j - \epsilon_a - \epsilon_b} g_{aibj}, \quad (7)$$

where we use a standard notation in which  $i, j \dots$  and  $a, b \dots$  run over HF occupied (occ) and virtual (vir) orbitals respectively.

Therefore, by choosing

$$D_{pq}^{\text{eff}} = D_{pq}^{\text{HF}}, \quad (8)$$

and

$$d_{pqrs}^{\text{eff}} = d_{pqrs}^{\text{HF}} + d_{pqrs}^{\text{MP2}}, \quad (9)$$

wherein

$$d_{pqrs}^{\text{MP2}} = \begin{cases} \frac{(2g_{pqrs} - g_{qrps})}{\epsilon_q + \epsilon_s - \epsilon_p - \epsilon_r} & \text{if } p \in \text{vir}, q \in \text{occ}, r \in \text{vir}, s \in \text{occ}, \\ 0 & \text{otherwise.} \end{cases} \quad (10)$$

we can recover the MP2 electronic energy with the aid of expression (4).

Due to the absence of  $d_{iijj}$  or  $d_{ijjj}$  matrix elements in  $\mathbf{d}^{\text{MP2}}$ , the effective MP2 second order reduced density matrix (2RDM) integrates to the HF first order RDM,  $\int \rho_2^{\text{eff}}(\mathbf{r}_1, \mathbf{r}_2; \mathbf{r}'_1, \mathbf{r}'_2) d\mathbf{r}_2|_{\mathbf{r}'_2 \rightarrow \mathbf{r}_2} = (N-1)\rho_1^{\text{HF}}(\mathbf{r}_1; \mathbf{r}'_1)$ . Notice that we are using McWeeny's normalization convention and spinless RDMs. This unrelaxed approach is not built upon a first-order response density, also known as the Handy-Schaefer Z-vector formalism,[29] as it has become standard in QTAIM/MP2 topological calculations. Thus, all one-electron properties and electron density based descriptors remain unchanged and equal to their HF values. Likewise, since the total second order reduced density (2RD) is the sum of its HF component plus the MP2 term, all Coulomb and exchange contributions are also unchanged with respect to their HF counterparts, and therefore

$$E_{\text{corr}}^{\text{MP2}} = \frac{1}{2} \sum_{iajb} d_{aibj} g_{iajb} = E_{\text{corr}}^{\text{self/MP2}} + E_{\text{corr}}^{\text{int/MP2}}. \quad (11)$$

The nature of Equation (11) allows for a very substantial saving in the computational effort needed to carry out an IQA calculation. All the standard implementations of IQA at the correlated level perform a monadic diagonalization of a matrix of size  $N(N+1)/2$ , where  $N = O + V$  is the total number of orbitals in the basis set, i.e., the sum of the occupied ( $O$ ) plus virtual ( $V$ ) spaces (see Ref. [30] for details). This diagonalization is also possible in the present approach, because the  $d_{aibj}$  matrix is symmetric,  $d_{aibj} = d_{bjai}$ .

The diagonalization procedure leads to the expression

$$\rho_2^{\text{eff}}(\mathbf{r}_1, \mathbf{r}_2) = \sum_{\mu} \lambda_{\mu} f_{\mu}(\mathbf{r}_1) f_{\mu}(\mathbf{r}_2), \quad (12)$$

with the functions  $f_{\mu}(\mathbf{r}_1)$  being the monadic eigenfunctions. Then, an expensive 6-dimensional

numerical integration is computed for each pair of functions  $f_\mu(\mathbf{r}_1)f_\mu(\mathbf{r}_2)$ . Therefore, methods which limit the orbital space (e.g. CASSCF), have been preferred up to now in IQA decompositions. However, we need herein only to integrate  $O(O + 1)/2$  monadic products which result from the HF state plus  $V \times O$  terms coming from the MP2 part, where  $V$  is the number of virtual orbitals. In typical MP2 calculations intended for real-life chemical problems,  $V \gg O$ , and the computational effort to calculate these six-dimensional integrals is thus reduced by a factor that scales as  $V/O$  in comparison with implementations based on integrals over atomic basis functions. [22, 26] This economical approach allows for significant reductions of the computational time required to perform the IQA analyses using MP correlated density functions.

### *Computational details*

We have carried out the IQA energy partition of the MP2 energy for a set of small molecules ( $\text{H}_2$ ,  $\text{H}_4$ ,  $\text{LiH}$ ,  $\text{BeH}_2$  and  $\text{BH}_3$ ) using a series of basis sets of different size, namely STO-3G [31], 6-31G [32, 33], 6-311G [34], cc-pVDZ, cc-pVTZ, aug-cc-pVDZ, aug-cc-pVTZ [35, 36], def2-SVPD, and def2-TZVP. [37] Additionally, we performed the IQA/MP2 analyses of (i) the ethane dimer, (ii) the  $\text{He}\cdots\text{Be}$ ,  $\text{He}\cdots\text{H}_2$ ,  $\text{Li}^+\cdots\text{He}$  and  $\text{Li}^+\cdots\text{H}_2$  van der Waals clusters and (iii) the formation of amine borane. All geometry optimizations were carried out using the ORCA [38] program at the MP2/aug-cc-pVTZ [35] level of theory employing the RIJCOSX approximation [39, 40] with the corresponding auxiliary basis sets. [41, 42] Density matrices were later obtained with the help of the PYSCF suite. [43] All electrons and orbitals were considered in these calculations. IQA integrations were performed using  $\beta$ -spheres with radii between 0.1 and 0.3 bohr. Restricted angular Lebedev quadratures with 5810 points and 451 points Gauss-Chebyshev mapped radial grids were used inside the  $\beta$ -spheres, with  $L$  expansions cut at  $l = 10$ . Outside the  $\beta$ -spheres, extended 5810-point Lebedev, 551- and 651- mapped radial point Gauss-Legendre quadratures, and  $L$  expansions up to  $l = 12$  were selected. All IQA calculations were done with our in-house code PROMOLDEN, available upon request. [44] [Total energies reconstructed by PROMOLDEN are accurate to less than a](#)

kcal/mol. As an example, the errors in the total MP2 energy with our IQA reconstruction for the  $\text{Li}^+ \cdots \text{H}_2$ ,  $\text{He} \cdots \text{Be}$ ,  $\text{He} \cdots \text{H}_2$ , and  $\text{Li}^+ \cdots \text{He}$  systems are 0.02, 0.002, 0.02, and 0.02 kcal/mol, respectively.

## Results and discussion

Figure 1 shows the comparison between computer times of IQA calculations that include all the MP2 matrix components and those considering only the  $VOVO$  elements of the two-electron matrix as established in Equation (10). The difference in computer time is noticeable even for systems with small basis sets and it becomes larger as the number of basis set functions increases.

We fitted the computer times of both algorithms of the IQA/MP2 calculations to the formula  $y = ax^n$  and obtained the values of  $n$ , which correspond to the scaling factor of each procedure. For the computations including all the 2-RDM matrix elements,  $n$  turns out to be around 4.27. In contrast, the scaling factor is reduced to 1.04 in the efficient implementation put forward in this paper, [with reasonable prefactors](#). In other words, by considering only the occupied to virtual elements we obtain almost a linear scaling. As reported in Figure 1, the computed times of the implementation reported are considerably reduced with respect to the previous methodology. For example, if the IQA-MP2 calculation of a system with 400 orbitals would require around one month of computer time using the traditional procedure, it now takes less than an hour with the algorithm here described. Thus, the proposed implementation paves the way to divide the MP2 correlation energy in atomic and interatomic contributions at a substantially lowered computational effort.

### *The ethane dimer*

The ethane dimer is an archetype in the study of hydrophobic interactions. The two ethane molecules are kept together by dispersion forces. In contrast to Hartree-Fock and many common exchange-correlation functionals, the MP2 approximation is able to describe this aggregate correctly. Thus, this system presents an interesting opportunity to investigate

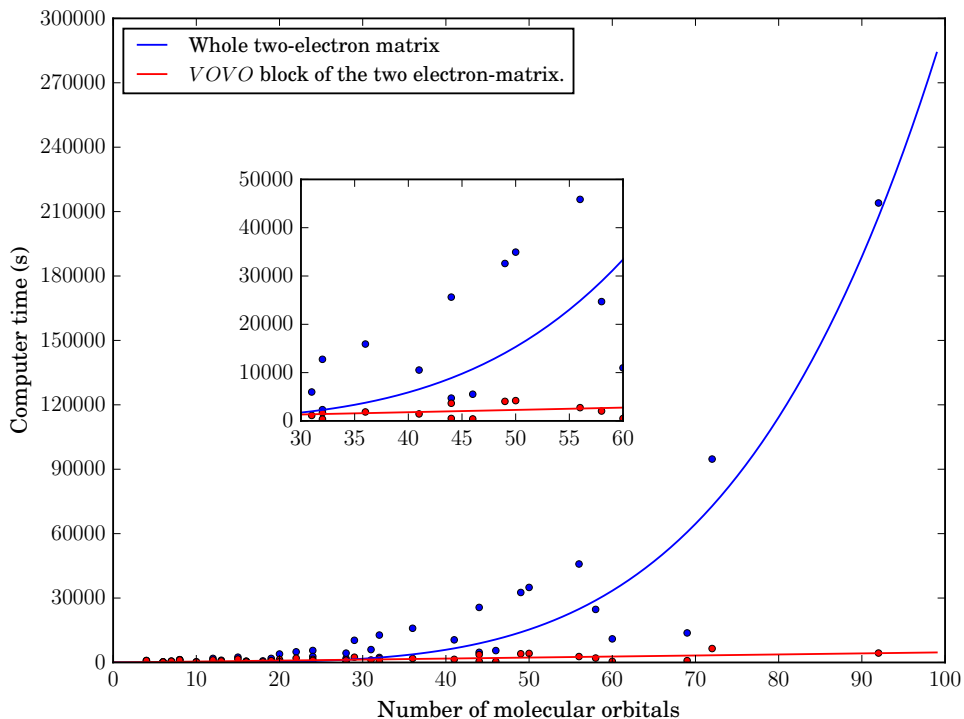


Figure 1: Computer times of IQA/MP2 calculations considering the whole two electron matrix  $\mathbf{d}$  (blue dots) and its *VOVO* block (red dots) as a function of the number of molecular orbitals in the Fock space. The lines correspond to  $y = ax^n$  fittings, see the main text for further details. All calculations were carried out using one core in a Intel i7-4790 3.60GHz processor and none required more than 1GB of RAM during execution.

interatomic interactions in hydrocarbon chains and it is therefore suitable to illustrate the method proposed herein.

We carried out the IQA/MP2 energy partition of the electronic energy of the ethane dimer in four different arrangements (a)-(d), as shown in Figure 2. Table 1 contains a summary of our results. The total IQA interaction energy is rather small, from  $-2.9$  to  $-12.4$  kcal/mol. Table 2 also reports the smallest C...C intermolecular distances. One might conjecture that such distances should be correlated with  $E_{\text{int}}^{\text{AB}}$ , but that is not the case. This circumstance occurs because the interaction energy between the  $\text{C}_2\text{H}_6$  molecules results from numerous intermolecular interactions in the system.

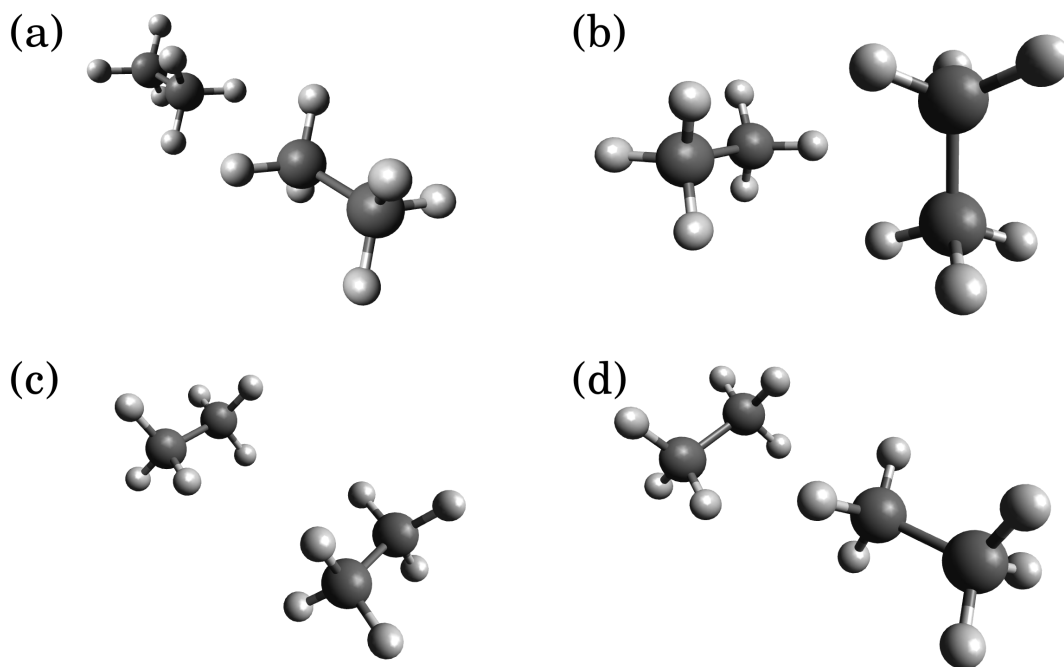


Figure 2: Different conformations of the ethane dimer addressed in this investigation: (a) facing each other, (b) cross-shaped, (c) side to side and (d) T-shaped. The IQA/MP2 computation of each monomer took around 260 hours of computer time.

Moreover, the role of the classical term in the formation of the complex is almost negligible. The value of the classical component of the interaction energy is larger than 0.2 kcal/mol in no case. This fact, however, does not mean that there are not specific stabilizing or destabilizing classical interactions between the atoms. For instance, there is a carbon-carbon classical destabilization in conformer (a) with a value as large as 2.6 kcal/mol. Nevertheless, these repulsions nearly cancel the attractive hydrogen-carbon interactions within the dimer.

The exchange-correlation term of the total interaction energy is the one responsible for stabilizing the complexes. This result occurs mainly because of the addition of the exchange-correlation of different contributions throughout the system. Indeed, the xc component of the interaction energy between the carbon atoms facing each other in conformer (a) amounts to only  $-0.7$  kcal/mol but the whole accounting of the carbon and hydrogen interactions equals  $-6.4$  kcal/mol.

Table 1: Partition of the interaction energy between  $C_2H_6$  molecules as well as the smallest distance between carbon atoms in the different conformations of the ethane dimer examined in this work (Figure 2). The superindices A and B refer to each ethane molecule within the complex. The energy values are reported in kcal/mol.

System	$E_{\text{int}}^{\text{AB}}$	$V_{\text{cl}}^{\text{AB}}$	$V_{\text{xc}}^{\text{AB}}$	$V_{\text{corr}}^{\text{AB}}$	C...C ( $\text{\AA}$ )
(a)	-6.3	0.1	-6.4	-1.1	3.56
(b)	-12.4	0.2	-12.6	-2.0	3.84
(c)	-2.9	0.1	-3.0	-0.7	4.53
(d)	-7.0	0.1	-7.1	-1.2	3.85

We can further examine the values of the exchange-correlation energy for different pairs of atoms in the four conformers of  $(C_2H_6)_2$  addressed herein (Table 2). As stated before, atomic pairwise values of the exchange-correlation energy are small and hence, the number of such contacts is critical in determining the strength of the whole interaction. Indeed, the H...H and C...H interactions play an important role in the formation of the investigated conformations of the ethane dimer.

Finally, the exchange-correlation energy between distant atoms can be identified with dispersion forces, as we have shown [21]. Although each individual interaction is weak, they are collectively important in establishing the structure of a system. For instance, dispersion forces are able to stabilize very long carbon-carbon bonds [45] and to force very short H...H intermolecular contacts. [46] An important factor in the energetics for the formation of the investigated dispositions of the ethane dimer is the number of atoms that are in close proximity, i.e., at a distance smaller than 5  $\text{\AA}$ . The most stable conformers of  $(C_2H_6)_2$  are found to be clearly related to those having the largest number of close intermolecular contacts as reported in Table 2.

Table 2: Average exchange-correlation energies for C...C, H...H and C...H intermolecular contacts that contribute more than 0.1 kcal/mol to the total interaction energy of the investigated structures of (C<sub>2</sub>H<sub>6</sub>)<sub>2</sub> (Figure 2). The number of such contacts is given in parentheses. The energy values are reported in kcal/mol.

System	$V_{XC}^{C...C}$	$V_{XC}^{H...H}$	$V_{XC}^{C...H}$
(a)	-0.68 (1)	-0.56 (9)	-0.41 (6)
(b)	-0.19 (3)	-1.71 (4)	-0.52 (9)
(c)	0.00 (0)	-0.38 (5)	-0.37 (2)
(d)	-0.23 (2)	-0.60 (7)	-0.40 (6)

*Bonding in small van der Waals clusters*

As discussed in the previous subsection, in order to properly describe systems held together by dispersion forces it is necessary to include electron correlation. We computed the MP2/aug-cc-pVQZ formation energy of four complexes, two that are bound only by dispersion forces (He...Be and He...H<sub>2</sub>) and other two that also include charge-induced multipole interactions (Li<sup>+</sup>...He and Li<sup>+</sup>...H<sub>2</sub>). This kind of systems have been successfully used as models of dispersion-bound systems. [47]

We found that the differences between the two types of interactions, purely dispersive and charge-induced, are conspicuously reflected in the structure and interatomic distances in the complexes, as shown in Figure 3. The equilibrium distance for the complexes that contain the ion Li<sup>+</sup> are much shorter (around 2 Å smaller) than those for the neutral clusters. This observation results, of course, from the large charge-induced multipole contributions in the Li<sup>+</sup>-containing clusters. We point out that the H<sub>2</sub> molecule does not form a linear complex with He and Li<sup>+</sup>. Instead, the three atoms of He...H–H form a 150° angle, while Li<sup>+</sup>...H<sub>2</sub> has a C<sub>2v</sub> structure at the MP2 level, as illustrated in Figure 3. Said structures are in agreement with previous reports. [48–51]

Regarding the formation energy of the the different complexes, the values corresponding to He...Be and He...H<sub>2</sub> are quite small, less than 1 kcal/mol, while the values for Li<sup>+</sup>...He

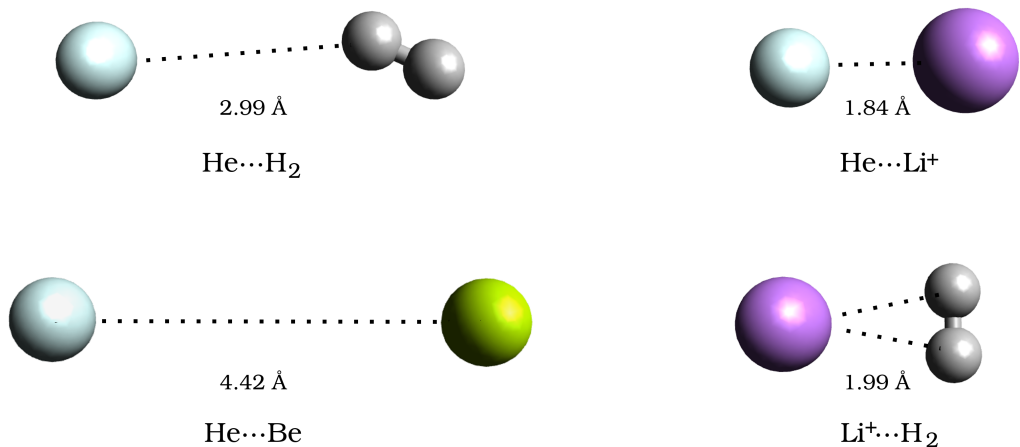


Figure 3: Structure of the  $\text{HeH}_2$ ,  $\text{HeLi}^+$ ,  $\text{HeBe}$  and  $\text{H}_2\text{Li}^+$  clusters.

and  $\text{Li}^+\cdots\text{H}_2$ , are substantially larger as expected (Table 3). Although the quantity  $\Delta E_{\text{form}}$  is considerably small for  $\text{He}\cdots\text{Be}$  and  $\text{He}\cdots\text{H}_2$  clusters ( $\Delta E_{\text{form}} \sim 10^{-2}$  kcal/mol), we note that the components of the IQA partition energy are one order of **magnitude** larger and therefore they are easier to compute with a good accuracy. This condition makes the IQA analysis of the adducts  $\text{He}\cdots\text{Be}$  and  $\text{He}\cdots\text{H}_2$  physically sound and meaningful. The IQA energy partition also shows that the neutral complexes have very small binding, interaction and deformation energies, **which are defined with respect to the energies of the fully optimized isolated fragments, e.g. the He atom and the  $\text{H}_2$  molecule.** Indeed, the formation of these complexes barely affects the electronic cloud of their constituent molecules.

Considering the division of the interaction energy into its classical and exchange-correlation terms, we can observe that there is practically no contribution from  $V_{\text{cl}}$  between the fragments for the neutral complexes and hence that all the interaction energy comes from the exchange-correlation term, as shown in Table 3.

Regarding the correlation energy, which Gonthier and Head-Gordon considered as central in the description of these systems, [47] we found unexpectedly that its role in this kind of interactions is secondary. The correlation component of  $V_{\text{xc}}$  is much smaller than that of exchange in all the clusters examined. However, this smaller role of the correlation for

the interaction energies could be related with the spatial distribution of  $E_{\text{corr}}$ , which in this case could be concentrated within the atoms and not in the intermolecular interactions, as we have discussed previously. [21] We emphasize however that in those cases where the interaction entails a molecule, i.e.,  $\text{He}\cdots\text{H}_2$  and  $\text{Li}^+\cdots\text{H}_2$ , the correlation term is much larger than those wherein only atoms are involved,  $\text{He}\cdots\text{Be}$  and  $\text{Li}^+\cdots\text{He}$ . This result could point towards a non-negligible role of the correlation energy in the description of atom-bond interactions, an important issue for the development of force fields in molecular dynamics. [52, 53]

Table 3: Equilibrium distances for the  $\text{He}\cdots\text{Be}$ ,  $\text{He}\cdots\text{H}_2$ ,  $\text{Li}^+\cdots\text{He}$  and  $\text{Li}^+\cdots\text{H}_2$  clusters and components of the IQA interaction energy. The values are reported in kcal/mol.

System	$R_{\text{eq}}$ (Å)	$E_{\text{form}}$	$E_{\text{def}}$	$E_{\text{int}}$	$V_{\text{cl}}$	$V_{\text{xc}}$	$V_{\text{x}}$	$V_{\text{corr}}$	XR
$\text{He}\cdots\text{Be}$	4.415	-0.02	0.33	-0.35	0.00	-0.35	-0.34	-0.01	-0.01
$\text{He}\cdots\text{H}_2$	3.180	-0.02	0.61	-0.63	0.00	-0.63	-0.54	-0.09	-0.04
$\text{Li}^+\cdots\text{He}$	1.838	-2.56	3.18	-5.74	-2.11	-3.63	-3.50	-0.13	-0.43
$\text{Li}^+\cdots\text{H}_2$	1.989	-7.39	5.99	-13.38	-7.06	-6.33	-6.07	-0.26	-0.31

We have added the total deformation energy to the exchange-correlation interaction component in Table 3 to form the so-called exchange-repulsion XR term,  $\text{XR} = E_{\text{def}}^A + E_{\text{def}}^B + V_{\text{xc}}^{AB}$ , where the two fragments in which we divide the systems are called  $A$  and  $B$ . Here, the value of XR is negative in all cases. This indicates that for the studied systems the covalent contribution to the bond compensates the energy associated with the deformation processes and points towards importance of including  $V_{\text{xc}}$  in the description of the systems. Recall that XR has been associated to the exchange-repulsion energy in perturbation treatments of intermolecular interactions. [54]

Finally, we indicate that the hydrogen molecule is much more affected than the helium atom by its interaction with the cation  $\text{Li}^+$ . This statement is based on the deformation energies of  $\text{H}_2$  and  $\text{He}$  upon forming the corresponding clusters. The value for  $\text{Li}^+\cdots\text{H}_2$  ( $E_{\text{def}}=5.99$  kcal/mol) is almost double the one associated to  $\text{Li}^+\cdots\text{He}$  ( $E_{\text{def}}=3.18$  kcal/mol). Although

the equilibrium distances of both complexes are very similar, the classical interaction of the system  $\text{Li}^+\cdots\text{H}_2$  is more than three times larger than it is in  $\text{Li}^+\cdots\text{He}$ . Both observations are in agreement with the larger polarizability of  $\text{H}_2$  with respect to that of He (He: 1.38 vs  $\text{H}_2$ : 1.53  $\text{\AA}^3$ .) and the smaller ionization potential for Helium (He: 24.6 eV vs  $\text{H}_2$ : 15.4 eV). Electrons are much more closely bound to the Helium nucleus than to the hydrogen molecule. Notice that although the He and  $\text{H}_2$  moieties are two-electron systems, the intermolecular exchange component is much larger in the latter system. This is again related to the larger spatial extension of  $\text{H}_2$  with respect to He, i.e. to the larger  $\text{Li}^+\text{-H}_2$  *overlap*.

### *Formation of ammonia borane*

We illustrate further the IQA/MP2 methodology put forward in this paper by examining ammonia borane,  $\text{H}_3\text{NBH}_3$ . One of the main features of this system is the electrostatic interaction between the nitrogen and boron atoms, which is systematically overestimated by the Hartree-Fock method. We have computed the potential energy curve for the formation of this molecule to get further insights about the interaction between N and B (Figure 4). The equilibrium distance ( $R_{\text{eq}}$ ) between these atoms is 1.58  $\text{\AA}$ , and the shape of the curve corresponds to a rather strong interaction.

The computed bond dissociation energy (BDE) for B–N in ammonia borane is about 33 kcal/mol, a value similar to the one of the  $\text{F}_2$  molecule (39 kcal/mol) and one third of that corresponding to the breaking of a carbon-carbon bond in a typical alkane. [55] The picture presented by the BDE of  $\text{H}_3\text{N-BH}_3$  is, however, not complete. Bond dissociation energies result from a compromise between the energy necessary to deform the isolated molecules to the configuration they exhibit in the complex, and the interaction energies between these contorted species. In the present case, the deformation energies of  $\text{NH}_3$  and  $\text{BH}_3$  are 116 and 67 kcal/mol, respectively and the interaction energy of these deformed species is  $-216$  kcal/mol (Table 4). These add to a BDE of  $-33$  kcal/mol.

We will focus now on the nature of the interaction energy between  $\text{NH}_3$  and  $\text{BH}_3$  in ammonia borane. Given the large QTAIM atomic charges of the B and N basins (2.12 and  $-1.25$

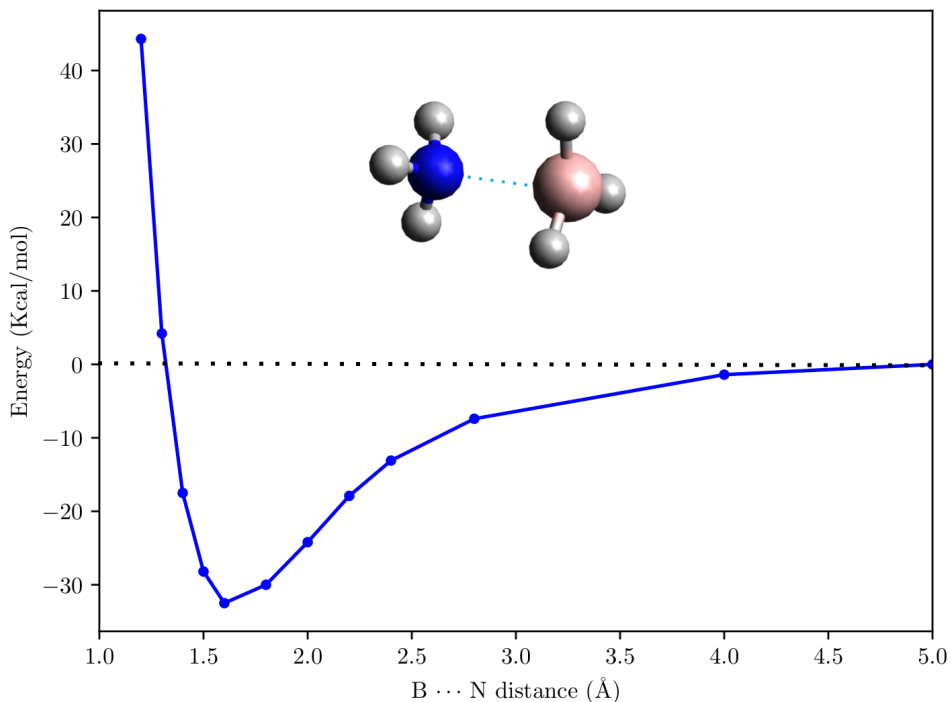


Figure 4: Relaxed surface scan corresponding to the potential energy curve for the formation on ammonia borane as a function of the B...N distance computed with the MP2/aug-cc-pVDZ approximation. The values are reported in kcal/mol. The IQA partition of each point required 20 hours of computer time.

Table 4: IQA/MP2 intermolecular contributions for the  $\text{H}_3\text{NBH}_3$  complex at the equilibrium distance. The values are reported in kcal/mol.

Property	$E_{\text{int}}$	$V_{\text{cl}}$	$V_{\text{xc}}$	$V_{\text{x}}$	$V_{\text{corr}}$	$E_{\text{def}}^{\text{NH}_3}$	$E_{\text{def}}^{\text{BH}_3}$	XR
Value	-216.1	-102.8	-113.3	-89.1	-24.2	116.2	67.5	94.6

atomic units respectively), one could expect the interaction energy between the ammonia and borane molecules to be dominated by electrostatics. Nevertheless, that is not the case. At the equilibrium geometry,  $E_{\text{int}}$  is almost evenly split into its classical and exchange-correlation components. The latter is even slightly larger in magnitude ( $-113$  kcal/mol) than the former

( $-103$  kcal/mol)<sup>1</sup> One of the reasons behind this counterintuitive fact is the different nature and decay rate of the classic and exchange correlation-energies. We have recently discussed this issue in detail. [57] The exchange-correlation energies are always attractive and therefore the contribution for the different pairs of atoms add up to the intermolecular attraction. On the contrary,  $V_{cl}$  can be either attractive or repulsive, and the overall charge neutrality condition usually leads to partial or complete cancellation. Figure 5 shows a scheme of the different electrostatic interactions occurring in the formation of the  $\text{H}_3\text{N}\cdots\text{BH}_3$  complex. The  $\text{B}\cdots\text{N}$  contact is large and stabilizing. Notwithstanding, the interaction between (i) boron and the hydrogens in ammonia and (ii) nitrogen and the hydrides in borane are destabilizing. Finally, the intermolecular interactions among hydrogen atoms is attractive. The total value of  $V_{cl}$  is obtained by adding these cancelling contributions.

Regarding the exchange-correlation term of the interaction energy between the fragments, our results show how it comes almost entirely from two contributions. The first one comes from electron delocalization between the boron and the nitrogen atoms. Nevertheless, more than 92 % of the total B–N interaction energy is classical. The other important contribution to the intermolecular exchange-correlation energy comes from the delocalization of electrons between the nitrogen atom and the hydrogens in borane. Finally, the splitting of the exchange and correlation energies in Table 4 shows that most of  $V_{xc}$  (80 %) arises from the exchange part and that only 20% comes from the correlation term. Nonetheless, the correlation energy ( $-24$  kcal/mol) is comparable to the BDE ( $-33$  kcal/mol) a result that highlights the importance of the inclusion of this term for the correct description of this system. Actually, the XR term ( $94.6$  kcal/mol) is now repulsive and is barely compensated by the classical interaction.

---

<sup>1</sup>Previously, some of us reported a value of  $V_{cl}$  for this system at a slightly different geometry of  $-72.2$  kcal/mol at the aug-cc-pVDZ/HF level of theory. [56] Our tests indicate that this difference comes from the different basis sets.

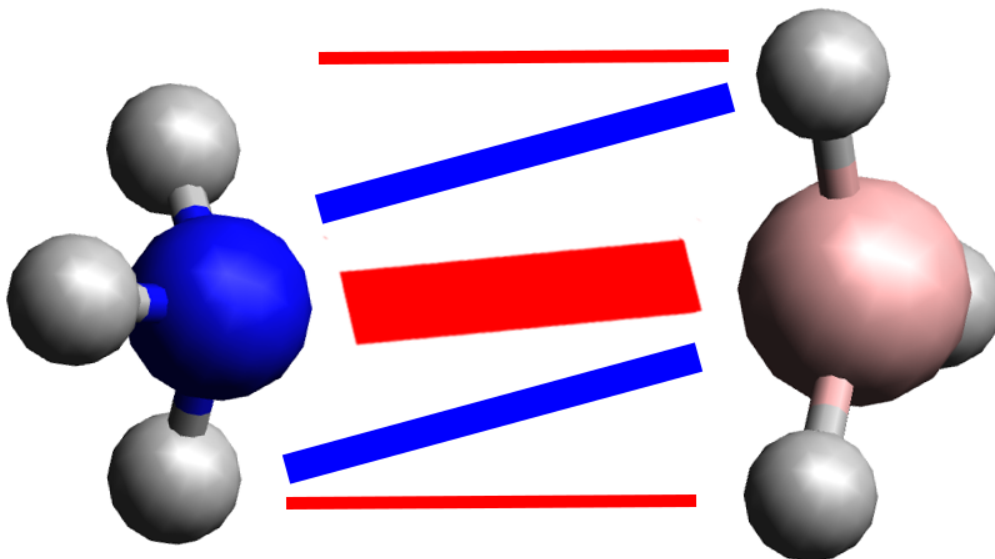


Figure 5: Qualitative representation of the electrostatic interactions occurring in the ammonia borane complex. The stabilizing/destabilizing interactions are coloured in red/blue.

## Conclusions

We have presented in this contribution a simple algorithmic improvement that achieves considerable computational gains in the Interacting Quantum Atoms partition of Møller-Plesset electronic energies. Our proposed implementation shows an almost linear scaling factor (1.04) with respect to the number of basis functions used in the molecular structure calculation. This scaling is in sharp contrast with that corresponding to the traditional IQA implementation which scales nearly as fourth power of  $N$ . This improvement allows for the study of larger systems with reduced computational effort for the real space partition of MP2 correlation energies. We have also considered several simple systems to illustrate the performance of the algorithm put forward herein. We expect that this improvement in the IQA/MP2 partition will prove useful to get insights about the effects of electron correlation in covalent and non-covalent interactions throughout physical chemistry.

## Acknowledgements

We thank the Spanish MICINN, grant PGC2018-095953-B-I00, the FICyt, grant IDI-2018-000177 and the European Union FEDER funds for financial support. J.M.G.V. and T.R.R. acknowledge financial support from CONACyT/Mexico (grant 253776) and PAPITT/UNAM (project IN205118). We are also thankful to DGTIC/UNAM for computer time (projects LANCAD-UNAM-DGTIC 250).

## References

- [1] M. A. Blanco, A. Martín Pendás, E. Francisco, *J. Chem. Theory Comput.* **2005**, *1*, 1096–1109.
- [2] E. Francisco, A. Martín Pendás, M. A. Blanco, *J. Chem. Theory Comput.* **2005**, *2*, 90–102.
- [3] R. F. W. Bader, *Atoms in molecules: A Quantum Theory*, Oxford University Press, **1990**.
- [4] A. Martín Pendás, M. A. Blanco, E. Francisco, *J. Chem. Phys.* **2006**, *125*, 184112.
- [5] J. M. Guevara-Vela, R. Chávez-Calvillo, M. García-Revilla, J. Hernández-Trujillo, O. Christiansen, E. Francisco, A. Martín Pendás, T. Rocha-Rinza, *Chem. Eur. J.* **2013**, *19*, 14304–14315.
- [6] J. M. Guevara-Vela, E. Romero-Montalvo, V. A. Mora Gómez, R. Chávez-Calvillo, M. García-Revilla, E. Francisco, A. Martín Pendás, T. Rocha-Rinza, *Phys. Chem. Chem. Phys.* **2016**, *18*, 19557–19566.
- [7] J. M. Guevara-Vela, E. Romero-Montalvo, A. Costales, A. Martín Pendás, T. Rocha-Rinza, *Phys. Chem. Chem. Phys.* **2016**, *18*, 26383–26390.
- [8] E. Romero-Montalvo, J. M. Guevara-Vela, A. Costales, A. Martín Pendás, T. Rocha-Rinza, *Phys. Chem. Chem. Phys.* **2017**, *19*, 97–107.
- [9] O. A. Syzgantseva, V. Tognetti, L. Joubert, *J. Phys. Chem. A* **2013**, *117*, 8969–8980.
- [10] K. Eskandari, M. Lesani, *Chem. Eur. J.* **2015**, *21*, 4739–4746.
- [11] J. M. Guevara-Vela, D. Ochoa-Resendiz, A. Costales, R. Hernández-Lamoneda, A. Martín Pendás, *ChemPhysChem* **2018**, *19*, 2512–2517.
- [12] A. Martín Pendás, E. Francisco, M. A. Blanco, C. Gatti, *Chem. Eur. J.* **2007**, *13*, 9362–9371.

- [13] D. Ferro-Costas, E. Francisco, A. Martín Pendás, R. A. Mosquera, *ChemPhysChem* **2016**, *17*, 2666–2671.
- [14] J. Jara-Cortés, J. M. Guevara-Vela, A. Martín Pendás, J. Hernández-Trujillo, *J. Comput. Chem.* **2017**, *38*, 957–970.
- [15] A. Fernández-Alarcón, J. L. Casals-Sainz, J. M. Guevara-Vela, A. Costales, E. Francisco, A. Martín Pendás, T. Rocha-Rinza, *Phys. Chem. Chem. Phys.* **2019**, *21*, 13428–13439.
- [16] D. Tiana, E. Francisco, M. A. Blanco, P. Macchi, A. Sironi, A. Martín Pendás, *J. Chem. Theory Comput.* **2010**, *6*, 1064–1074.
- [17] D. Tiana, E. Francisco, M. A. Blanco, P. Macchi, A. Sironi, A. Martín Pendás, *Phys. Chem. Chem. Phys.* **2011**, *13*, 5068.
- [18] E. Romero-Montalvo, J. M. Guevara-Vela, W. E. Vallejo Narváez, A. Costales, A. Martín Pendás, M. Hernández-Rodríguez, T. Rocha-Rinza, *Chem. Commun.* **2017**, *53*, 3516–3519.
- [19] Z. Badri, C. Foroutan-Nejad, J. Kozelka, R. Marek, *Phys. Chem. Chem. Phys.* **2015**, *17*, 26183–26190.
- [20] C. Foroutan-Nejad, Z. Badri, R. Marek, *Phys. Chem. Chem. Phys.* **2015**, *17*, 30670–30679.
- [21] J. L. Casals-Sainz, J. M. Guevara-Vela, E. Francisco, T. Rocha-Rinza, A. Martín Pendás, *ChemPhysChem* **2017**, *18*, 3553–3561.
- [22] J. L. McDonagh, A. F. Silva, M. A. Vincent, P. L. A. Popelier, *J. Phys. Chem. Lett.* **2017**, *8*, 1937–1942.
- [23] P. L. Bora, M. Novák, J. Novotný, C. Foroutan-Nejad, R. Marek, *Chem. Eur. J.* **2017**, *23*, 7315–7323.
- [24] R. Chávez-Calvillo, M. García-Revilla, E. Francisco, A. Martín Pendás, T. Rocha-Rinza, *Comput. Theor. Chem.* **2015**, *1053*, 90–95.
- [25] F. J. Holguín-Gallego, R. Chávez-Calvillo, M. García-Revilla, E. Francisco, A. Martín Pendás, T. Rocha-Rinza, *J. Comput. Chem.* **2016**, *37*, 1753–1765.
- [26] J. L. McDonagh, M. A. Vincent, P. L. Popelier, *Chem. Phys. Lett.* **2016**, *662*, 228–234.
- [27] M. A. Vincent, A. F. Silva, P. L. A. Popelier, *J. Comput. Chem.* **2019**, *40*, 2793–2800.
- [28] I. Ruiz, E. Matito, F. J. Holguín-Gallego, E. Francisco, A. Martín Pendás, T. Rocha-Rinza, *Theor. Chem. Acc.* **2016**, *135*.

- [29] N. C. Handy, H. F. Schaefer, *J. Chem. Phys.* **1984**, *81*, 5031–5033.
- [30] A. Martín Pendás, E. Francisco, M. A. Blanco, *J. Comput. Chem.* **2005**, *26*, 344–351.
- [31] M. S. Gordon, J. S. Binkley, J. A. Pople, W. J. Pietro, W. J. Hehre, *J. Amer. Chem. Soc.* **1982**, *104*, 2797–2803.
- [32] W. J. Hehre, R. Ditchfield, J. A. Pople, *J. Chem. Phys.* **1972**, *56*, 2257–2261.
- [33] J. D. Dill, J. A. Pople, *J. Chem. Phys.* **1975**, *62*, 2921–2923.
- [34] R. Krishnan, J. S. Binkley, R. Seeger, J. A. Pople, *J. Chem. Phys.* **1980**, *72*, 650–654.
- [35] R. A. Kendall, T. H. Dunning, R. J. Harrison, *J. Chem. Phys.* **1992**, *96*, 6796–6806.
- [36] B. P. Prascher, D. E. Woon, K. A. Peterson, T. H. Dunning, A. K. Wilson, *Theor. Chem. Acc.* **2010**, *128*, 69–82.
- [37] F. Weigend, R. Ahlrichs, *Phys. Chem. Chem. Phys.* **2005**, *7*, 3297–3305.
- [38] F. Neese, *Wiley Interdiscip. Rev. Comput. Mol. Sci.* **2017**, *8*, e1327.
- [39] F. Neese, F. Wennmohs, A. Hansen, U. Becker, *Chem. Phys.* **2009**, *356*, 98–109.
- [40] S. Kossmann, F. Neese, *J. Chem. Theory Comput.* **2010**, *6*, 2325–2338.
- [41] F. Weigend, A. Köhn, C. Hättig, *J. Chem. Phys.* **2002**, *116*, 3175–3183.
- [42] F. Weigend, *Phys. Chem. Chem. Phys.* **2006**, *8*, 1057.
- [43] Q. Sun, T. C. Berkelbach, N. S. Blunt, G. H. Booth, S. Guo, Z. Li, J. Liu, J. D. McClain, E. R. Sayfutyarova, S. Sharma, S. Wouters, G. K.-L. Chan, *Wiley Interdiscip. Rev. Comput. Mol. Sci.* **2017**, *8*, e1340.
- [44] A. Martín Pendás, E. Francisco, *Promolden. A QTAIM/IQA code (unpublished)*.
- [45] S. Rösel, H. Quanz, C. Logemann, J. Becker, E. Mossou, L. Cañadillas-Delgado, E. Caldeweyher, S. Grimme, P. R. Schreiner, *J. Amer. Chem. Soc.* **2017**, *139*, 7428–7431.
- [46] P. R. Schreiner, L. V. Chernish, P. A. Gunchenko, E. Y. Tikhonchuk, H. Hausmann, M. Serafin, S. Schlecht, J. E. P. Dahl, R. M. K. Carlson, A. A. Fokin, *Nature* **2011**, *477*, 308–311.

- [47] J. F. Gonthier, M. Head-Gordon, *J. Chem. Phys.* **2017**, *147*, 144110.
- [48] I. Hayes, G. Hurst, A. Stone, *Mol. Phys.* **1984**, *53*, 107–127.
- [49] P. Muchnick, A. Russek, *J. Chem. Phys.* **1994**, *100*, 4336–4346.
- [50] A.-M. Sapse, A. Dumitra, D. C. Jain, *J. Clust. Sci.* **2003**, *14*, 21–30.
- [51] C. Emmeluth, B. L. J. Poad, C. D. Thompson, G. H. Weddle, E. J. Bieske, *J. Chem. Phys.* **2007**, *126*, 204309.
- [52] F. Pirani, M. Albertí, A. Castro, M. M. Teixidor, D. Cappelletti, *Chem. Phys. Lett.* **2004**, *394*, 37–44.
- [53] E. Estrada, *Chem. Phys. Lett.* **2008**, *463*, 422–425.
- [54] A. Martín Pendás, M. A. Blanco, E. Francisco, *J. Comput. Chem.* **2009**, *30*, 98–109.
- [55] S. J. Blanksby, G. B. Ellison, *Acc. Chem. Res.* **2003**, *36*, 255–263.
- [56] J. J. Novoa (Ed.), *Intermolecular Interactions in Crystals*, The Royal Society of Chemistry, **2018**.
- [57] A. Martín Pendás, E. Francisco, *Phys. Chem. Chem. Phys.* **2018**, *20*, 21368–21380.